ACS EARTH AND SPACE CHEMISTRY

http://pubs.acs.org/journal/aesccq

Article

Atmospheric Oxidation of Propanesulfinic Acid Initiated by OH Radicals: Reaction Mechanism, Energetics, Rate Coefficients, and Atmospheric Implications

Parandaman Arathala and Rabi A. Musah*

Cite This: *ACS Earth Space Chem.* 2021, 5, 1498−1510

Read Online

ACCESS | Metrics & More | Article Recommendations | Supporting Information

ABSTRACT: The atmospheric oxidation mechanism and energetics of propanesulfinic acid ($CH_3CH_2CH_2S(O)OH$, PSIA) initiated by OH radicals have been investigated at the CCSD(T)/aug-cc-pVTZ//M06-2X/aug-cc-pVTZ level of theory. The PSIA + $^{\bullet}$OH reaction proceeds through (i) H-atom abstraction and (ii) $^{\bullet}$OH addition pathways. The calculated energies indicate that the barrier height for the abstraction of H-atom from the −OH moiety of PSIA leading to the formation of $CH_3CH_2CH_2S(O)_2$ + H_2O is estimated to be −4.7 kcal mol^{-1} relative to that of the separated reactants. The rate coefficients were determined for all possible reaction paths by RRKM-ME calculations using Master equation solver for multienergy well reactions (Mesmer) code in the atmospherically relevant temperatures between 200 and 320 K and bath gas pressures between 0.1 and 10 atm. The calculated bimolecular rate coefficients suggest that the formation of $CH_3CH_2CH_2S(O)_2$ + H_2O is predominant compared to the other possible reaction paths in the studied temperature range. The total rate coefficient for the PSIA + $^{\bullet}$OH reaction was found to be ∼8.40 × 10^{-11} cm^3 molecule^{-1} s^{-1} at T = 298 K and P = 1 atm. In addition, branching ratios, thermochemical parameters, atmospheric lifetime, and global warming potentials were determined. Overall, the results indicate that the atmospheric removal of PSIA with $^{\bullet}$OH results in the formation of sulfur dioxide (SO_2) from C−S single bond fission in the CH_3−CH_2−CH_2−$S(O)_2$ radical, which is formed by H-atom abstraction from the OH group of PSIA. Thus, the SO_2 product does not originate from the direct elimination of SO_2 from unimolecular dissociation of PSIA. The formed SO_2, propylene (C_3H_6), sulfurous acid (H_2SO_3), and hydroperoxyl (HO_2) radical are major products that may contribute to global warming and aerosol formation.

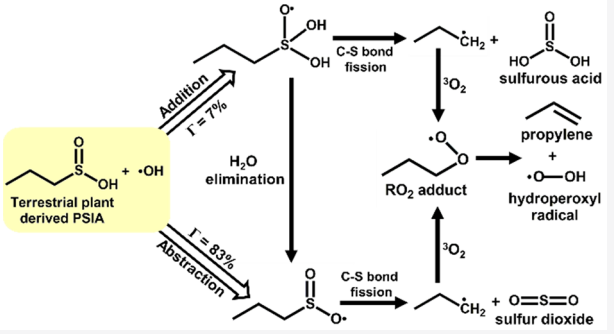

KEYWORDS: *propanesulfinic acid, OH radical, barrier height, rate coefficient, branching ratio, atmospheric lifetime, global warming potential, sulfur dioxide*

1. INTRODUCTION

Many volatile organosulfur compounds (VOSCs) released into the atmosphere have attracted great interest because they play important roles in global warming, acid precipitation, and cloud formation and contribute to the global sulfur budget.[1−4] Dimethyl sulfide (DMS, CH_3SCH_3) is the most abundant biogenic sulfur compound and is released in large quantities from the oceans by oceanic phytoplankton.[5] DMS is emitted predominantly by marine environments, whereas hydrogen sulfide (H_2S), DMS, methanethiol (CH_3SH), carbon disulfide (CS_2), carbonyl sulfide (OCS), and several other species are produced from terrestrial emissions.[2] It has been suggested that DMS and other VOSCs play a major role in atmospheric aerosol and cloud formation.[6,7] In addition, a number of studies have reported that dimethyl thiosulfinate (CH_3−$S(O)S$−CH_3), dipropyl thiosulfinate ($CH_3CH_2CH_2$−$S(O)S$−$CH_2CH_2CH_3$), propyl methyl thiosulfinate, diphenyl thiosulfinate, and several other VOSCs are emitted from various *Allium* genus cash crops such as garlic and onions that occupy large acreage on farmlands.[8,9] This raises the question of whether the farming of these crops and their emission of VOSCs into the atmosphere results in organosulfur "hotspots" that may have a significant effect on global warming, Earth's climate, the environment, and human health. Recently reported computational investigations of the atmospheric oxidation of dipropyl thiosulfinate (DPTS) with hydroxyl (OH) radical[10] and dimethyl thiosulfinate (DMTS) with $^{\bullet}$OH/$^{\bullet}$Cl[11] suggest that while the global warming potentials of DMTS and DPTS are themselves negligible, the numerous products formed as a consequence of their interactions with $^{\bullet}$OH and $^{\bullet}$Cl may make

Received: March 7, 2021
Revised: April 14, 2021
Accepted: April 25, 2021
Published: May 17, 2021

substantial contributions to global warming, acid rain, and formation of secondary organic aerosols.

One such molecule is propanesulfinic acid (PSIA, $CH_3-CH_2-CH_2-S(O)-OH$), an important trace compound that was recently reported to be a product of the oxidation of plant-derived DPTS with OH radicals via the addition of •OH to the S-atom of the sulfinyl moiety, followed by S(=O)−S single bond cleavage.[10] According to this study, the formation of PSIA is a major reaction path with a total contribution of ∼60−80% at the tropospheric temperatures between 200 and 300 K. Thus, DPTS plant emissions could lead to substantial release of PSIA into the atmosphere, which raises the question of what the atmospheric removal process might be for this molecule. Since OH radicals control the removal of VOSCs, volatile organic compounds (VOCs), and other trace gases from the earth's atmosphere,[12−15] we have investigated the atmospheric removal process of PSIA with OH radicals to better understand its atmospheric fate. This radical is a highly reactive and short-lived species with a daytime average concentration of $\sim 10^6$ molecule cm^{-3} under typical tropospheric conditions.[16]

The fate of sulfinic acids in the atmosphere is expected to be dominated by their reactions with OH radicals. Yet, there are no reports on the atmospheric removal of PSIA with •OH. However, there have been various theoretical and experimental studies on the atmospheric reactions of methanesulfinic acid (MSIA) with •OH.[17−20] Kukui et al.[19] have studied the reaction of MSIA + •OH using a high-pressure turbulent flow reactor coupled to an ion molecule reaction mass spectrometer. They reported that the dominant reaction path of MSIA + •OH involved the formation of the $CH_3S(O)_2$ radical, followed by its rapid decomposition via C−S single bond cleavage to form sulfur dioxide (SO_2). The rate coefficient for the MSIA + •OH reaction was reported to be $(9 \pm 3) \times 10^{-11}$ cm^3 $molecule^{-1}$ s^{-1} at 298 K and P = 200−400 Torr. Later, the mechanism of the atmospheric oxidation of MSIA + •OH was studied by González-García et al.[18] using theoretical calculations at the CCSD(T)/IB//mPW1K/MG3S level. The possible abstraction and addition−elimination channels were investigated, and their corresponding rate coefficients were calculated using variational transition-state theory (VTST). This study concluded that the abstraction of H-atom by •OH leading to the formation of the $CH_3S(O)_2$ radical with a water molecule was a major path. The global rate coefficient for this reaction at 298 K was reported as 7.7×10^{-10} cm^3 $molecule^{-1}$ s^{-1}. In another study, Tian et al.[17] investigated the various possible reaction paths for MSIA + •OH at the CCSD(T)/6-311+G(2d,p)//B3LYP/6-31+G(2d,p) level. Their findings also suggested that •OH association with MSIA, followed by decomposition leading to the formation of $CH_3S(O)_2 + H_2O$, is a feasible reaction path.

Compared to MSIA, which has a single methyl group with 3 equivalent hydrogens bound to carbon, the situation with PSIA is a bit more complex because the presence of the propyl group provides more sites with which the •OH can interact. Reactions of •OH with PSIA can proceed through H-atom abstraction from the methylene and methyl moieties leading to the formation of the corresponding C-centered radicals and a water molecule. There are three different H-abstraction pathways for the formation of C-centered radicals (eqs 1−3)

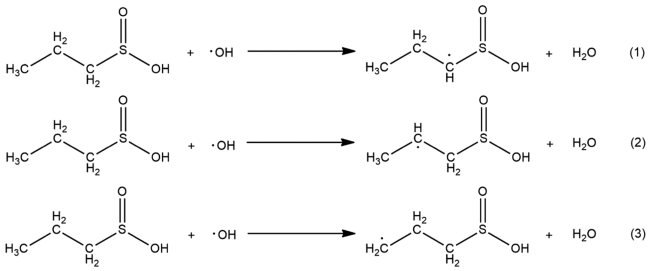

The other possible abstraction reaction proceeds through removal of the H-atom from the −OH moiety of PSIA by •OH, leading to the formation of the $CH_3CH_2CH_2S(O)_2$ radical and a water molecule (eq 4)

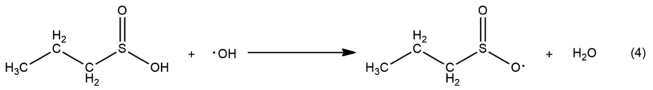

A similar mechanism was suggested by González-García et al.[18] and Kukui et al.[19] for the formation of $CH_3S(O)_2$ from the MSIA + •OH reaction. In addition, the formation of this product may proceed not only by direct H-atom abstraction from the −OH moiety of MSIA but also by the addition of •OH to the S-atom followed by elimination of water. We considered an analogous pathway by which the PSIA + •OH reaction leads to the formation of $CH_3CH_2CH_2S(O)_2$ as a radical product. The reaction initially proceeds via the addition of •OH to the S-atom of PSIA, which leads to formation of the $CH_3CH_2CH_2S(O)(OH)_2$ radical, followed by elimination of a water molecule (eqs 5 to 6)

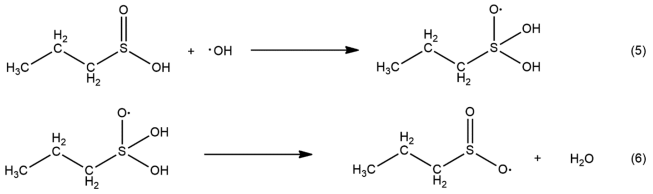

In a study reported by Flyunt et al.,[20] of the MSIA + •OH reaction in aqueous solution using a pulse radiolysis technique, it is suggested that •OH reacts preferentially by addition, which is then followed by fragmentation. We also proposed a similar mechanism for the PSIA + •OH reaction. The formed product $CH_3CH_2CH_2S(O)(OH)_2$ radical undergoes further decomposition via C−S single bond cleavage (see eq 7) leading to the formation of a propyl radical and sulfurous acid (H_2SO_3)

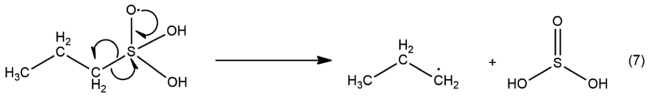

To the best of our knowledge, no study has been reported to date on the reaction mechanism, energetics, and rates for the reaction of PSIA with •OH. To learn about the atmospheric fate of PSIA, a more complete understanding of the reaction mechanism is very important. Therefore, the possible H-abstraction and •OH addition pathways involved in the PSIA + •OH reaction were investigated using ab initio/DFT electronic structure calculations. The transition states corresponding to possible intermediates such as pre- and postreactive complexes were located to identify and characterize the reaction pathways. The rate coefficients of all of the possible reaction paths were calculated using Mesmer[21] kinetic code in the atmospherically relevant temperature range of 200−320 K and

https://doi.org/10.1021/acsearthspacechem.1c00062
ACS Earth Space Chem. 2021, 5, 1498−1510

a pressure range of 0.1−10 atm. The atmospheric implications of the PSIA + •OH reaction were explored by determining the branching ratios. The overall results of this work further contribute to a better understanding of the chemistry of sulfinic acids in the atmosphere.

2. COMPUTATIONAL METHODS

The Gaussian16 software package[22] was used to perform all of the quantum chemistry calculations involving the atmospheric oxidation of PSIA initiated by •OH. The stationary point geometries on the potential energy surfaces (PESs) for the PSIA + •OH reaction were fully optimized using the DFT method. The present DFT calculations were carried out at the M06-2X hybrid meta density functional[23] and in conjunction with an augmented correlation-consistent triplet-zeta basis set (aug-cc-pVTZ).[24] This method was found to be suitable for developing the reaction mechanisms and estimating the rate coefficients for various atmospheric reactions.[25−27] Intrinsic reaction coordinate (IRC)[28,29] calculations were performed to confirm that all of the pre- and postreactive complexes belonged to the corresponding transition states (TSs). Harmonic vibrational frequencies were calculated at the same level of theory to verify the nature of the corresponding TSs or stable minima, like the reactants, pre- and postreactive complexes, and products. All of the positive vibrational frequencies suggest that for stable minima, all of the TSs must have a single imaginary frequency. The final energies were estimated by performing single-point energy calculations at the coupled cluster singles and doubles, augmented by a perturbative treatment of triple excitation ((CCSD(T)) level[30] coupled with the same aug-cc-pVTZ basis set on the geometries optimized at the same M06-2X/aug-cc-pVTZ level. The total electronic energies (E_{total}) along with the zero-point energy (ZPE)-corrected electronic energies [E_{total}(ZPE)] of the reactants, pre- and postreactive complexes, TSs, and products obtained at the M06-2X and CCSD(T) levels are given in Table S1. Normal mode vibrational frequencies at the M06-2X/aug-cc-pVTZ level were performed to estimate the respective zero-point energy corrections for the stable minima and TSs. The computed E_{total}(ZPE) corrections for the CCSD(T) level used the ZPE associated with the M06-2X/aug-cc-pVTZ level calculations. The optimized geometries, and the imaginary frequencies of the various TSs, rotational constants, and vibrational frequencies, are provided in Tables S2−S5. We also estimated the T1 diagnostic for the CCSD(T) calculations[31] to verify the multireference character of the wave functions of all of the stationary points involved in this work. The corresponding values are displayed in Table S6 of the Supporting Information. The data from the table indicate that the T1 values for all of the species were <0.02, except for SO_2 and the transition state (TS10). This indicates that a single reference-based electron correlation procedure was suitable for the present calculations.

3. RESULTS AND DISCUSSION

We first present the detailed description of the electronic structure calculations and energetics of the various possible pathways in the PSIA + •OH reaction. We then present and analyze the rate coefficients calculated for each individual channel using the ab initio/DFT-determined PESs, and this is followed by an estimation of the overall rate coefficients. To investigate the present PSIA + •OH reaction mechanism, we began by performing a conformational analysis of PSIA to find the most stable conformer. The structure of PSIA involves four internal rotational degrees of freedom (two C−C, one C−S, and one O−S). The dihedral angles for the corresponding rotations can be identified as H10C8C3S1, H12C11C8C3, H5C3S1O2, and H7O6S1O2, respectively. The various structures of the conformers were fully optimized at the M06-2X/aug-cc-pVTZ level, and the five most stable conformations based on their energies are presented in Figure 1. The optimized geometries of the stable structures for PSIA

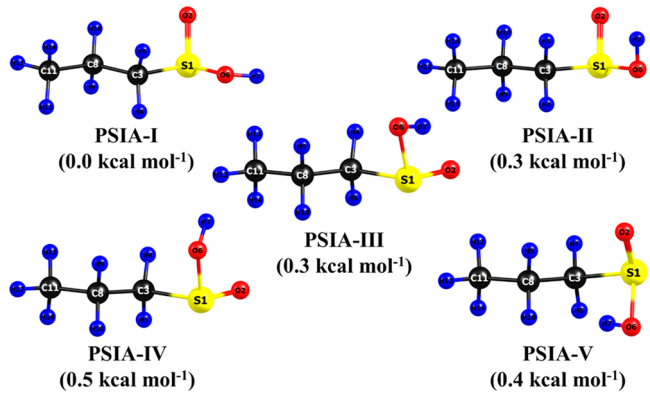

Figure 1. M06-2X/aug-cc-pVTZ level-optimized conformational structures of propanesulfinic acid (PSIA). The energies are the zero-point-corrected relative energies computed at the CCSD(T)/aug-cc-pVTZ//M06-2X/aug-cc-pVTZ level.

are labeled as PSIA-I, PSIA-II, PSIA-III, PSIA-IV, and PSIA-V. The structures PSIA-II and PSIA-IV are rotational isomers of PSIA-I by the internal rotation of the O6−H7 and C3−H4 bonds around the S1−O2 axis, respectively. The energies calculated at the CCSD(T)//M06-2X level for all of the conformers presented in Figure 1 suggest that PSIA-I is the most stable (~0.3−0.5 kcal mol^{-1}) compared to the other possible conformers. The relative position of the OH group with respect to S(=O) for the most stable conformer of PSIA-I is in good agreement with that of the structure of MSIA reported in the literature.[17,32,33] Therefore, only the stable conformer (PSIA-I) was considered in the present calculations to study the reaction mechanism of PSIA with OH radicals under atmospheric conditions.

The geometry optimization and frequency calculations for these five conformers were performed using the B3LYP method coupled with the aug-cc-pV(T+d)Z basis set. This was done because the energies of the stable conformers were found to be very close (see Figure 1) and the presence of a sulfur atom in PSIA requires the triple-zeta basis set with additional tight d functions to properly describe its electronic structure.[34] The energies of all of the conformers determined at the B3LYP/aug-cc-pV(T+d)Z level were further refined by performing single-point energy calculations at the CCSD(T)/aug-cc-pV(T+d)Z level. The ZPE-corrected energies of all of the conformers were calculated relative to the energy of the most stable conformer of PSIA-I at the CCSD(T)/aug-cc-pV(T+d)Z//B3LYP/aug-cc-pV(T+d)Z level. The computed energies were compared with the values obtained at the CCSD(T)/aug-cc-pVTZ//M06-2X/aug-cc-pVTZ level, and the values are provided in Table 1. The data from the table indicate that the energy difference between all of the conformers at the CCSD(T)/aug-cc-pVTZ//M06-2X/aug-cc-

https://doi.org/10.1021/acsearthspacechem.1c00062
ACS Earth Space Chem. 2021, 5, 1498−1510

Table 1. Calculated Energies (in kcal mol^{-1}) of Various Conformers of Propanesulfinic Acid (PSIA) Computed at Two Different Levels of Theory

	ΔE (kcal mol^{-1})	
conformer	CCSD(T)/aug-cc-pVTZ//M06-2X/aug-cc-pVTZ	CCSD(T)/aug-cc-pV(T+d)Z//B3LYP/aug-cc-pV(T+d)Z
PSIA-I	0.0	0.0
PSIA-II	0.3	0.4
PSIA-III	0.3	0.3
PSIA-IV	0.5	0.6
PSIA-V	0.4	0.3

pVTZ level is ∼0.1 kcal mol^{-1} compared to the values obtained at the CCSD(T)/aug-cc-pV(T+d)Z//B3LYP/aug-cc-pV(T+d)Z level. The energies displayed in Table 1 at both levels suggest that the structure of conformer (PSIA-I) is more stable than the other possible conformers.

3.1. H-Atom Abstraction Pathways. The reaction of PSIA with •OH can proceed via two different classes of reactions: (1) direct H-atom abstraction and (2) addition of •OH to the S-atom of the −S(═O) moiety. The step-by-step details of these two classes were investigated using computational calculations performed at the CCSD(T)/aug-cc-pVTZ//M06-2X/aug-cc-pVTZ level. In PSIA, there are seven hydrogen atoms located on the C3, C8, and C11 atoms of the propyl ($CH_3-CH_2-CH_2-$) group and one on the O6 atom of −OH (see Figure 1). The optimized transition-state energies computed at the M06-2X/aug-cc-pVTZ level suggested only seven different TSs for the available eight H-atoms. This is because abstraction of the two hydrogen atoms linked to the C8-atom of the propyl moiety was found to have the same energy and were therefore considered as a single TS. All other hydrogens located on C3, C11, and O6 are distinct, which provides six different TSs. This gives a total of seven different H-abstraction TSs, which were labeled as TS1 and TS2 for C3; TS3 for C8; TS4, TS5, and TS6 for C11; and TS7 for the O6 atom-linked hydrogens. The seven different hydrogen abstraction TSs are labeled on the H-atoms involved in the structure of PSIA shown below.

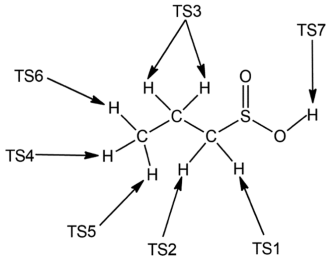

The M06-2X/aug-cc-pVTZ-optimized geometries and the potential energy profiles for all possible H-abstraction pathways involved in the PSIA + •OH reaction are shown in Figures 2 and 3, respectively. The energies of all of the stable minima are displayed in Figure 3, and they were calculated at the CCSD(T)/aug-cc-pVTZ//M06-2X/aug-cc-pVTZ level. The structures clearly show that •OH can abstract the H-atoms present in the propyl and −OH moieties attached to the sulfinyl S-atom of PSIA. The present calculations suggest that the abstraction of the two H-atoms linked to C8 of the propyl group has the same energy and that all of the other H-atoms (at −C3, −C11, and −O6) are different. The PESs shown in Figure 3 indicate that all of the H-atom abstraction channels start from the separated reactants (PSIA + •OH). The two

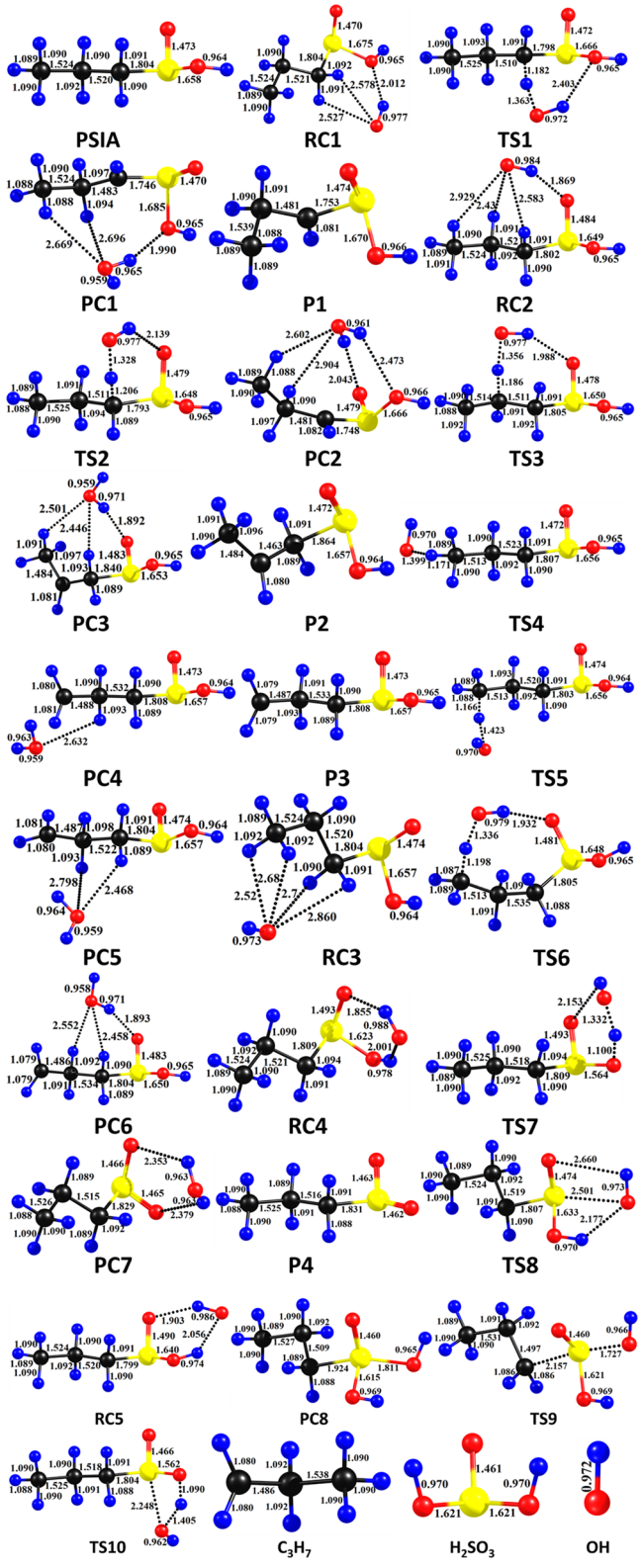

Figure 2. M06-2X/aug-cc-pVTZ level-optimized geometries of the reactants, prereactive complexes (RCs), transition states (TSs), postreactive complexes (PCs), and products for all of the possible paths involved in the propanesulfinic acid with •OH reaction. The yellow, black, blue, and red colors represent sulfur, carbon, hydrogen, and oxygen atoms, respectively.

reactants associate to form stable prereactive complexes (RCs). These then proceed via their corresponding TSs to the

https://doi.org/10.1021/acsearthspacechem.1c00062
ACS Earth Space Chem. 2021, 5, 1498−1510

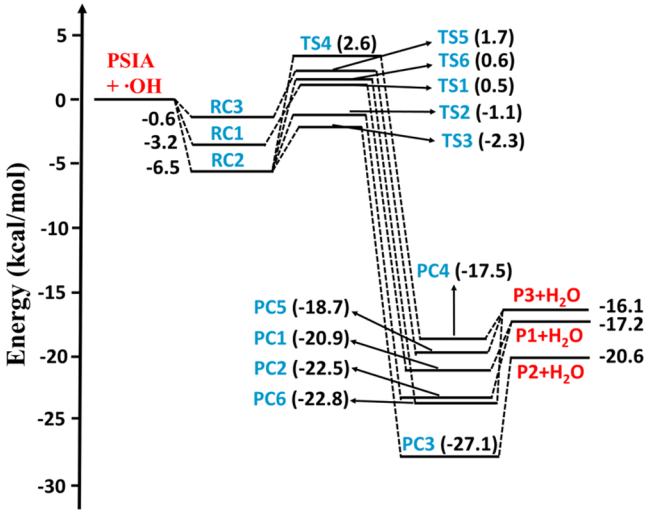

Figure 3. Potential energy profiles for the H-atom abstraction paths involved in the propanesulfinic acid (PSIA) with •OH reaction leading to the formation of the corresponding C-centered radical and water molecule products. Energies of the stationary points were obtained at the CCSD(T)/aug-cc-pVTZ//M06-2X/aug-cc-pVTZ level. The relative energies include zero-point corrections. The symbols RCn (n = 1−3) refer to prereactive complexes; TSn (n = 1−6) refer to transition states; and PCn (n = 1−6) refer to postreactive complexes.

formation of the corresponding postreactive complexes (PCs) and then finally to form their products. The RCs and PCs were observed at the entrance and exit channels of each H-atom abstraction pathway (see Figure 3). These stable complexes were found by optimizing the final structures of the reactant and product sides from the IRC calculations. This procedure was followed for searching the RCs and PCs for all of the TSs. In this process, we found more than one H-abstraction path leading to the same RC. From Figure 3, association of the two reactants (PSIA and •OH) in the entrance channels of the PES initially proceeds to form three different stable RCs (RC1, RC2, and RC3) with binding energies of ∼−3.2, ∼−6.5, and ∼−0.6 kcal mol^{-1} respectively, relative to the starting reactants. The stability of these three RCs is due to the formation of hydrogen-bonding interactions between the H- and O-atoms of PSIA with the O- and H-atoms of •OH, respectively (see Figure 2). The H-bond distances in these three complexes (RC1, RC2, and RC3) were found to be in the range between 1.87 and 2.86 Å. The H-atom abstraction proceeds from RC1, where the OH radical is oriented in such a way that it abstracts the H-atom linked to the C3-atom of PSIA via a six-membered ring-like transition state (TS1), with a barrier height of ∼0.5 kcal mol^{-1} above that of the starting reactants. This leads to the formation of PC1 with a stabilization energy of −20.9 kcal mol^{-1} and then on to form bimolecular products (P1 ($CH_3CH_2C^{\bullet}HS(O)(OH)$) + H_2O) at −17.2 kcal mol^{-1}. The other H-atom present on the C3-atom of PSIA is abstracted by •OH via RC2 and which leads to the formation of a six-membered ring-like transition state (TS2) with a barrier height of ∼−1.1 kcal mol^{-1} relative to that of the starting reactants. The formed TS2 further proceeds via the formation of PC2, which is stabilized at −22.5 kcal mol^{-1}, and then to the same final products (P1 + H_2O). Abstraction of H-atoms from the C3-atom by •OH through TS2 was found to have a ∼1.6 kcal mol^{-1} smaller barrier than it would have had if it proceeded via TS1. In the case of H-atoms linked to the C8-atom, our M06-2X calculations suggest that each hydrogen abstraction requires the same energy and therefore we considered them as reacting along a single path. The reaction continues from RC2 and then to the formation of TS3 with a barrier height of −2.3 kcal mol^{-1} below that of the starting reactants. This reaction further continues to form PC3 with a binding energy of −27.1 kcal mol^{-1}, which then undergoes unimolecular decomposition to form P2 ($CH_3C^{\bullet}HCH_2S(O)$-(OH)) + H_2O as final products at −20.6 kcal mol^{-1} below the starting reactants. The other remaining three H-atoms are located on C11, and each H-atom abstraction path leads to a different TS. The two H-atom abstraction pathways proceed via the same RC2, which then leads to the formation of transition states (TS4 and TS6) with barrier heights of ∼2.6 and 0.6 kcal mol^{-1} above that of the starting reactants, respectively. These reactions further proceed via the corresponding PC4 and PC6 with corresponding energies of −17.5 and −22.8 kcal mol^{-1}, respectively. The formed PC4 and PC6 further proceed to the formation of products as P3 (i.e., ($C^{\bullet}H_2CH_2CH_2S(O)(OH)$) + H_2O) at −16.1 kcal mol^{-1} relative to that of the starting reactants. Similarly, the other remaining H-atom abstraction by OH radicals continues via RC3, which then passes through TS5 with a barrier height of 1.7 kcal mol^{-1}. The reaction then forms PC5 with a stabilization energy of −18.7 kcal mol^{-1} and then to the same P3 + H_2O final products. Therefore, the PESs presented in Figure 3 clearly suggest that the abstraction path that proceeds via TS3 is more dominant when compared to all other possible abstraction channels for the H-atoms attached to the propyl group.

The remaining abstraction pathway for the PSIA + •OH reaction is the abstraction of the H-atom from the OH moiety of PSIA. The CCSD(T)//M06-2X-calculated PES profile for this reaction path is presented in Figure 4. The mechanism for this reaction was found to proceed through a prereactive complex (RC4) with a binding energy of −8.6 kcal mol^{-1} below that of the starting reactants. The formed RC4 further proceeds through a saddle point structure (TS7) with a barrier

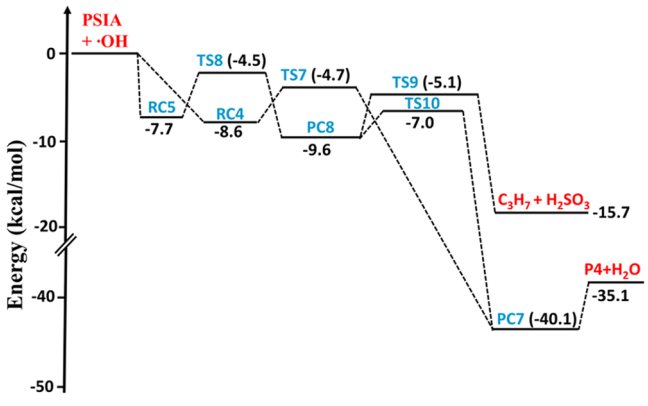

Figure 4. Potential energy profiles for the H-atom abstraction from the OH moiety of PSIA and the OH radical addition involved in the propanesulfinic acid + •OH reaction leading to the formation of the corresponding products. The energies of the stationary points were calculated at the CCSD(T)/aug-cc-pVTZ//M06-2X/aug-cc-pVTZ level. The relative energies include zero-point corrections. The symbols RCn (n = 4, 5), TSn (n = 7−10), and PCn (n = 7, 8) refer to prereactive complexes, transition states, and postreactive complexes, respectively.

https://doi.org/10.1021/acsearthspacechem.1c00062
ACS Earth Space Chem. 2021, 5, 1498−1510

height of ∼−4.7 kcal mol^{-1} below that of the starting reactants. The structure of TS7 (see Figure 2) shows that the OH radical-initiated abstraction occurs through a six-membered ring TS, which is stabilized by hydrogen-bonding interactions. The reaction then continues from TS7 by connecting with PC7 in the exit channel, with a stabilization energy of ∼40.1 kcal mol^{-1}. The formed PC7 undergoes unimolecular dissociation to form the final products ($CH_3CH_2CH_2S(O)_2$ (P4) + H_2O at −35.1 kcal mol^{-1}). In the present work, the energetics of all of the H-abstraction channels indicate that the abstraction of the H-atom from the OH moiety of PSIA via TS7 is predominant when compared to all other possible abstraction paths.

3.2. Addition−Dehydration Reaction. The steps of the PSIA + •OH reaction that proceed via the addition−dehydration mechanism are shown in eqs 5 and 6. The corresponding PES profiles and stationary point energies calculated at the CCSD(T)//M06-2X level are shown in Figure 4. In this mechanism, the association of •OH with the sulfinyl sulfur atom of PSIA leads to the formation of a prereactive complex (RC5) with an energy of ∼−7.7 kcal mol^{-1} below that of the reactants. The reaction proceeds from RC5 to TS8 with a barrier height of ∼−4.5 kcal mol^{-1} relative to that of the starting reactants. The reaction continues further to the formation of an addition product $CH_3CH_2CH_2S(O)$-$(OH)_2$ (PC8), which is −9.6 kcal mol^{-1} below the energy of the reactants. The TS energies on the PESs shown in Figure 4 indicate that the OH radical addition to the PSIA via TS8 has a barrier that is only ∼0.2 kcal mol^{-1} higher than the value for H-abstraction via TS7. This suggests that both reactions compete with one another. The formed PC8 undergoes elimination of a water molecule through the formation of a transition state (TS10) with a barrier height of −7.0 kcal mol^{-1}. PC7 forms from TS10, which then proceeds to P4 products (i.e., $CH_3CH_2CH_2S(O)_2$ + H_2O). We also found that PSIA + •OH can undergo an addition−elimination mechanism. This reaction also proceeds via RC5, TS8, and PC8. The formed PC8 undergoes elimination of propyl radical through TS9 with a barrier energy of ∼−5.1 kcal mol^{-1} relative to the separated reactants. The formed TS9 leads to the formation of propyl radical (C_3H_7) + sulfurous acid (H_2SO_3) as products via addition−elimination. The energies of the stationary points on the PES were found to be below the energy of TS8 for the elimination of propyl radical through PC8 and TS9 to form C_3H_7 + H_2SO_3. This was also observed to be true for the elimination of water through PC8 and TS10 to form $CH_3CH_2CH_2S(O)_2$ (P4) + H_2O. Thus, these two paths were found to be favorable under normal atmospheric conditions.

3.3. Direct Elimination of Sulfur Dioxide (SO_2). In addition to the various aforementioned pathways for the PSIA + •OH reaction in the atmosphere, we performed calculations for the unimolecular decomposition of PSIA via direct elimination of SO_2 to form propane. The PES surface involving all of the stationary point energies calculated at the CCSD(T)//M06-2X level is presented with respect to the starting reactant in Figure S1. From the figure, the reaction proceeds directly to the formation of a transition state (TS11) with a barrier height of ∼61.0 kcal mol^{-1}. The structure of TS11 shows the simultaneous transfer of the H-atom from the −OH moiety to the carbon atom of $-CH_2$ concomitant with the C−S(=O) single bond fission, leading to the formation of a postreactive complex (PC9), which then undergoes dissociation to form propane (C_3H_6) + SO_2. The barrier height for this reaction clearly indicates that while this pathway might be accessible in a high-temperature combustion scenario, direct SO_2 elimination is not important under normal atmospheric conditions. Hence, the rate coefficients for this reaction were not calculated.

The IRC plot was obtained at the M06-2X/aug-cc-pVTZ level for the unimolecular decomposition of PSIA through a transition state (TS11) to form SO_2 + propane, as shown in Figure S2. The structures presented from left to right in the IRC plot suggest that C−S single bond fission, H-atom transfer from the OH group to the C-atom of the propyl moiety, and double bond formation between the S- and O-atoms occur simultaneously before reaching the transition state on the reaction coordinate. The completion of single and double bond formations between the migrated H-atom and the C-atom of the propyl moiety and in the SO_2 moiety, respectively, occurs after reaching the transition state. This can be clearly seen by examining the structures given in the IRC plot shown in Figure S2.

The changes in enthalpy (ΔH) and Gibbs free energy (ΔG) at 298 K for all of the stationary points involved in all possible H-atom abstraction, OH addition, and direct SO_2 elimination pathways associated with the PSIA + •OH reaction were calculated at the CCSD(T)/aug-cc-pVTZ//M06-2X/aug-cc-pVTZ level, and the corresponding values are displayed in Table 2. The abstraction of H-atom from the −OH group of PSIA leading to the formation of $CH_3CH_2CH_2S(O)_2$ + H_2O for the TS7 abstraction channel was found to be more spontaneous compared to that of all possible reaction paths. The changes in enthalpy (ΔH) and Gibbs free energy (ΔG) for the TS7 abstraction channel were calculated to be −35.1 and −36.2 kcal mol^{-1}, respectively. This clearly indicates that the abstraction of H-atom from the −OH group of PSIA is more exothermic and highly favored compared to that of all other PSIA + •OH reaction paths.

3.4. Theoretical Kinetic Analysis. Master equation calculations were performed for the atmospheric oxidation of PSIA with •OH via various possible H-atom abstraction and •OH addition pathways (see eqs 1−5) using the Master equation solver for multienergy well reactions (MESMER v.5.2) code.[21] A detailed description of MESMER has been described in our previous work[10,11] and studies from various research groups.[21,35−37] We provide a brief discussion here for the Mesmer rate coefficient calculations. This kinetic code uses an energy-grained master equation approach in which the rotational−vibrational (rovibrational) energy states for all of the stationary points (such as reactants, TSs, RCs, PCs, and products on the PES for all possible reaction channels involved in the PSIA + •OH reaction) are partitioned into several energy grains, which contain a defined number of states. The energy states of initial reactants (PSIA + •OH) are allocated with populations using a Boltzmann distribution, and the other remaining species for the same reaction system are set to a population of zero. The change in population distribution between the energy states (grains) can take place over the reaction course in each reaction path through the collisional energy transfer that is due to the interaction with buffer gas and the interconversion of one species to another.

3.5. Rate Coefficients. The input parameters such as vibrational frequencies, rotational constants, and zero-point-corrected energies for the Mesmer rate calculations were obtained from the present theoretical work. The rate

https://doi.org/10.1021/acsearthspacechem.1c00062
ACS Earth Space Chem. 2021, 5, 1498−1510

Table 2. Enthalpies (ΔH (298 K) in kcal mol^{-1}) and Free Energies (ΔG (298 K) in kcal mol^{-1}) of the Various Stationary Points Involved in the PSIA + $^{\bullet}$OH Reaction Calculated at the CCSD(T)/aug-cc-pVTZ//M06-2X/aug-cc-pVTZ Level[a]

system	ΔH (298 K)	ΔG (298 K)
PSIA + OH	0.0	0.0
RC1	−3.5	4.1
TS1	−0.2	8.6
PC1	−20.5	−14.2
P1 + H_2O	−16.8	−18.7
RC2	−7.1	1.6
TS2	−2.1	7.6
PC2	−22.5	−14.7
TS3	−3.3	6.3
PC3	−27.0	−19.9
P2 + H_2O	−20.1	−22.0
TS4	2.1	10.0
PC4	−16.8	−12.6
P3 + H_2O	−15.5	−17.8
RC3	−0.6	6.1
TS5	1.1	9.3
PC5	−18.2	−12.5
TS6	−0.6	9.4
PC6	−22.6	−15.7
RC4	−9.4	−0.3
TS7	−5.7	3.9
PC7	−40.4	-32.5
P4 + H_2O	−35.1	-36.2
RC5	−8.3	0.1
TS8	−5.5	4.0
PC8	−10.6	−0.7
TS9	−10.7	−0.8
TS10	−6.4	3.8
H_2SO_3 + C_3H_7	−15.9	−19.2
TS11	60.9	60.9
PC9	−3.6	−7.4
C_3H_8 + SO_2	−2.4	−14.2

[a]The enthalpic (H) and free energy (G) corrections were derived from the M06-2X/aug-cc-pVTZ level calculations.

coefficients for the H-atom abstraction and $^{\bullet}$OH addition pathways were calculated in the temperature range of 200−320 K and a pressure range of 0.1−10 atm. The reaction mechanism proceeds through seven H-atom abstraction pathways and one $^{\bullet}$OH addition pathway. The PES profiles (see Figures 3 and 4) for all of the pathways suggest that they occur via three main steps: (1) the association of two reactants initially proceeds to form barrierless prereactive complexes; (2) the transition states with a well-defined barrier are formed between their corresponding pre- and postreactive complexes; and (3) the formation of products from decomposition of the corresponding postreactive complexes through the barrierless exit channel. The entrance channel (step 1) and exit channel (step 3) occur through barrierless reactions. Calculation of the rate coefficients for barrierless reactions is quite complicated due to the absence of a barrier along the minimum energy path, and thus it requires variational calculations. However, the variational treatment depends strongly upon the accurate determination of the minimum energy path and the level of theory used in the calculations.[35,38] Therefore, Mesmer offers the choice of calculating the microcanonical rate coefficients ($k(E)$) using the inverse Laplace transform (ILT) approach for the barrierless reactions. The Arrhenius pre-exponential factors (A) used in the ILT method in the present calculations were 1.0×10^{-10} and 1.0×10^{-11} cm^3 molecule^{-1} s^{-1} for the entrance and exit channels of the H-atom abstraction and $^{\bullet}$OH addition channels, respectively. The activation energy and the modified Arrhenius parameters used in rate calculations were 0 kcal mol^{-1} and 0.1, respectively. Reaction step 2 involving the transition of RCs to PCs through TSs uses the RRKM theory. The present rate calculations employed the Eckart tunneling[39] method to assess the tunneling contribution to the rate coefficients of all of the possible reaction paths in the studied temperature range.

Lennard-Jones (L-J) parameters (ε and σ) are required in Mesmer rate coefficient calculations. The depth of the potential well (ε) and the finite length, where the potential is zero (σ) for the RCs and PCs involved in all of the PESs, and the buffer gas, were taken from the literature. The buffer gas used in the present calculations was (N_2), with L-J parameters σ = 3.9 Å and ε = 48 K.[21] All of the pre- and postreactive adducts were assumed to have the same L-J parameters as n-heptane with σ = 4.42 Å and ε = 306.5 K.[40] These values were used because of the similarity of the size of all of the adducts to that of n-heptane. In addition, we tested our rate calculations by varying the L-J parameters for the n-octane and n-hexane and observed that the changes in the values were less than a factor of 2. Energy transfer was treated with the collision energy-transfer model for all of the PSIA + $^{\bullet}$OH reaction pathways, and the value was set to $\langle \Delta E_d \rangle$ = 200 cm^{-1}. This value was chosen based on similar reactions of $^{\bullet}$OH with other

Table 3. Calculated Bimolecular Rate Coefficients (in cm^3 molecule^{-1} s^{-1}) for All of the Possible H-Atom Abstraction and $^{\bullet}$OH Addition Pathways Involved in the PSIA + $^{\bullet}$OH Reaction in the Temperatures between 200 and 320 K and a Pressure of 1 atm

T (K)	k_{TS1}	k_{TS2}	k_{TS3}	k_{TS4}	k_{TS5}	k_{TS6}	k_{TS7}	k_{TS8}	k_{total}[a]
200	7.18×10^{-13}	4.78×10^{-12}	7.24×10^{-12}	6.00×10^{-15}	3.78×10^{-14}	2.30×10^{-12}	9.35×10^{-11}	2.37×10^{-11}	1.40×10^{-10}
220	5.91×10^{-13}	3.98×10^{-12}	6.58×10^{-12}	8.40×10^{-15}	4.37×10^{-14}	1.52×10^{-12}	8.94×10^{-11}	1.51×10^{-11}	1.24×10^{-10}
240	5.10×10^{-13}	3.32×10^{-12}	5.96×10^{-12}	1.15×10^{-14}	5.11×10^{-14}	1.01×10^{-12}	8.47×10^{-11}	9.39×10^{-12}	1.11×10^{-10}
250	4.81×10^{-13}	3.05×10^{-12}	5.67×10^{-12}	1.34×10^{-14}	5.54×10^{-14}	8.30×10^{-13}	8.23×10^{-11}	7.36×10^{-12}	1.05×10^{-10}
260	4.57×10^{-13}	2.80×10^{-12}	5.39×10^{-12}	1.55×10^{-14}	6.01×10^{-14}	6.90×10^{-13}	7.98×10^{-11}	5.77×10^{-12}	1.00×10^{-10}
280	4.22×10^{-13}	2.38×10^{-12}	4.88×10^{-12}	2.04×10^{-14}	7.06×10^{-14}	4.90×10^{-13}	7.46×10^{-11}	3.55×10^{-12}	9.12×10^{-11}
298	4.02×10^{-13}	2.08×10^{-12}	4.46×10^{-12}	2.59×10^{-14}	8.14×10^{-14}	3.75×10^{-13}	6.98×10^{-11}	2.32×10^{-12}	8.40×10^{-11}
320	3.88×10^{-13}	1.78×10^{-12}	4.02×10^{-12}	3.39×10^{-14}	9.62×10^{-14}	2.84×10^{-13}	6.39×10^{-11}	1.42×10^{-12}	7.60×10^{-11}

[a]The overall rate coefficient (k_{total}) for the PSIA + $^{\bullet}$OH reaction was calculated by summing the values for all of the individual reaction pathways at the corresponding temperature. The contribution of the rate coefficients via k_{TS3} was multiplied by 2.

https://doi.org/10.1021/acsearthspacechem.1c00062
ACS Earth Space Chem. 2021, 5, 1498−1510

atmospheric compounds.[10,11,41,42] After inputting all of the model parameters discussed above into Mesmer, the temperature- and pressure-dependent rate coefficients for all of the bimolecular reaction paths involved in the PSIA + •OH reaction were extracted from the eigenvalues of a corresponding Master equation by employing the Bartis−Widom method[43−46] developed in the MESMER kinetic code.[21]

The rate coefficients (in cm^3 $molecule^{-1}$ s^{-1}) given in Table 3 were calculated in the temperature range of 200−320 K and a pressure of 1 atm. The rate coefficients in Table 3 (represented as k_{TSn} (n = 1−8)) correspond to each H-atom abstraction and •OH addition path that proceeds via TSn (n = 1−8) in the PSIA + •OH reaction. It is clear from Table 3 that the rate coefficient values for the abstraction of H-atom via TS4 and TS5 increase with an increase in temperature, while the other reaction paths that proceed via TS1, TS2, TS3, TS6, TS7, and TS8 decrease and are slightly independent of temperature. This trend in the rate coefficient values is because the reactions that occur via TS4 and TS5 have positive TS barriers, while the reactions that proceed through TS2, TS3, TS7, and TS8 exhibit negative barriers, with slightly positive barriers for reactions arising via TS1 and TS6. The rate coefficients for the reaction paths that proceed via TS2, TS3, TS7, and TS8 decrease with increasing temperature. This decrease occurs because of the formation of a prereactive complex and the influence that the presence of the prereactive complex at the entrance channel of the PES has on the dynamics and hence the course of the reaction.[47,48] The presence of a prereactive complex for these reactions leads to rate coefficients with a negative temperature dependence. The role of such complexes has been extensively studied for the OH reaction with formic acid, ethene, acetone, and acetaldehyde.[47−50] These studies explain the role of prereactive complexes in which the bimolecular reaction rate coefficients are associated with a negative temperature dependence.

It is also clear from Table 3 that abstraction of the H-atom linked to the C8-carbon of the propyl group, which occurs via TS3, is more dominant by a factor of ∼2−14 times when compared to that of TS1 and TS2, and ∼10^1−10^3 times that for TS4 and TS5, respectively, in the studied temperatures for all possible H-atom abstractions from the propyl moiety of PSIA. The reason for the larger rate coefficients for TS3 is that its barrier height is ∼1.2−5.0 kcal mol^{-1} lower than that for the other possible H-atom abstractions from the propyl moiety of PSIA. Comparison of the rate coefficient values for all possible H-atom abstractions from both the propyl and −OH moieties of PSIA suggests that the H-atom abstraction from −OH that occurs via TS7 is ∼1−4 orders of magnitude larger than the values of the other abstraction paths. In addition, we have also calculated the rate coefficient for the addition of •OH to the S-atom of the sulfinyl group of PSIA, which proceeds through TS8. The estimated rate coefficients (k_{TS8}), which are also displayed in Table 3, suggest that this reaction is ∼4−45 times slower than the H-atom abstraction reaction (k_{TS7}). For example, the rate coefficients for the H-atom abstraction and •OH addition via TS7 and TS8 at 298 K and 1 atm were found to be k_{TS7} = 6.98 × 10^{-11} and k_{TS8} = 2.32 × 10^{-12} cm^3 $molecule^{-1}$ s^{-1}, respectively. The rate coefficient data suggest that abstraction of the H-atom from the −OH group of PSIA is kinetically more dominant compared to all possible H-atom abstraction and OH addition pathways.

In addition, we calculated the contributions from Eckart tunneling[39] to the rate coefficients for each reaction path and the values are displayed in Table S7 of the Supporting Information. The results in Table S7 suggest that the tunneling contributions to the rate coefficients for k_{TS3} and k_{TS6} are independent of temperature, whereas those for k_{TS1}, k_{TS2}, k_{TS4}, k_{TS5}, and k_{TS7} were increased by ∼2−9 times in the studied temperature range. The estimation of tunneling contributions to the rate coefficients for the addition channel (k_{TS8}) was found to be increased by ∼2−4 times in the studied temperature range (see Table S7).

The rate coefficients for all of the possible reaction paths were also calculated by varying the buffer gas pressure in the range of 0.1, 1.0, and 10 atm in the same temperature range between 200 and 320 K. The obtained bimolecular rate coefficient values are displayed in Tables 3 and S8 and S9 of the Supporting Information. The values indicate that the H-atom abstraction and addition pathways show very weak pressure dependences in the entire studied temperature range.

The overall rate coefficient (k in cm^3 $molecule^{-1}$ s^{-1}) is determined by adding each reaction path rate coefficient at the corresponding temperature. Therefore, the overall rate coefficient for the PSIA + •OH reaction is defined as k = k_{TS1} + k_{TS2} + 2k_{TS3} + k_{TS4} + k_{TS5} + k_{TS6} + k_{TS7} + k_{TS8}. Here, k_{TSn} (n = 1−8) designates the H-atom abstraction and •OH addition paths involved in the present reaction system. The contribution of rate coefficients for the H-atom abstraction via TS3 was multiplied by a factor of 2 in the overall rate coefficient calculations since the abstraction of each of the two H-atoms linked to the C8-carbon atom of PSIA exhibits the same energy. Therefore, we considered a single abstraction transition state for these two H-atoms. The obtained overall rate coefficient for the PSIA + •OH reaction in the studied temperature and pressure ranges was plotted. The result is shown in Figure 5, and the values are also provided in Tables 3 and S8 and S9 of the Supporting Information. It is clear from Figure 5 that the overall rate coefficient trends at 0.1, 1.0, and 10 atm show little pressure dependence in the studied temperature range. For example, the overall rate coefficients for the PSIA + •OH reaction at 250 K as the buffer gas pressure was varied in the range of 0.1, 1.0, and 10 atm were calculated to be 9.86 × 10^{-11}, 1.05 × 10^{-10}, and 1.29 × 10^{-10} cm^3 $molecule^{-1}$ s^{-1}, respectively.

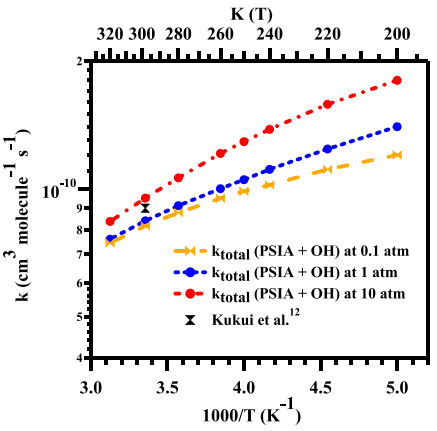

Figure 5. Comparison between the overall rate coefficients calculated for the PSIA + •OH reaction in the temperatures between 200 and 320 K and pressures between 0.1 and 10 atm. The available rate coefficient for the MSIA + •OH reaction at 298 K is also shown for comparison.

https://doi.org/10.1021/acsearthspacechem.1c00062
ACS Earth Space Chem. 2021, 5, 1498−1510

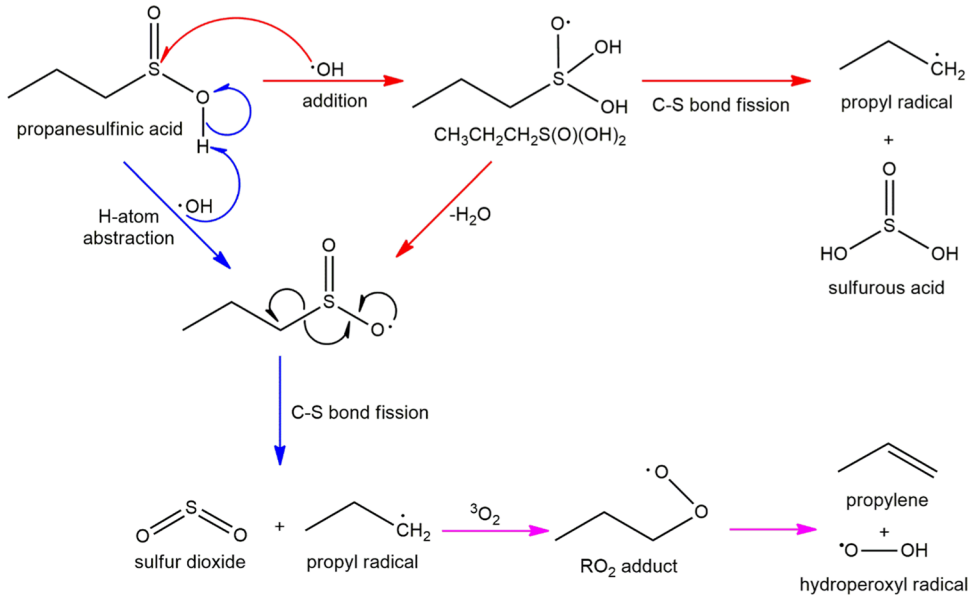

Figure 6. Proposed atmospheric degradation mechanism for the propanesulfinic acid initiated by OH radicals. The reaction proceeds through H-atom abstraction from the OH moiety of PSIA, leading to the formation of the $CH_3{-}CH_2{-}CH_2{-}S(O)_2$ radical + H_2O. The formed $CH_3{-}CH_2{-}CH_2{-}S(O)_2$ radical then undergoes C−S bond fission to form SO_2 + propyl radical (indicated with blue arrows). In an alternate pathway, the addition of $^{\bullet}OH$ to PSIA leads to the formation of the $CH_3{-}CH_2{-}CH_2{-}S(O)(OH)_2$ radical, which then undergoes elimination of water to form $CH_3{-}CH_2{-}CH_2{-}S(O)_2$ radical. In another pathway, the same $CH_3{-}CH_2{-}CH_2{-}S(O)(OH)_2$ radical undergoes C−S bond fission leading to the formation of propyl radical + sulfurous acid (indicated with red arrows). Finally, the formed propyl radicals can rapidly react with atmospheric oxygen ($^3O_2$), leading to the formation of an RO_2 adduct, which then undergoes unimolecular elimination of HO_2 radical to form propylene (indicated with pink arrows).

There are no reports available that enable us to compare our calculated overall rate coefficients for the PSIA + $^{\bullet}OH$ reaction. Therefore, our calculated rate coefficients were compared with the value for the MSIA + $^{\bullet}OH$ reaction reported in the literature. The overall rate coefficient value for the PSIA + $^{\bullet}OH$ reaction at 298 K and 1 atm was calculated to be ∼8.40 × 10^{-11} cm^3 $molecule^{-1}$ s^{-1}, which agrees very well with the measured rate coefficient for the MSIA + $^{\bullet}OH$ reaction reported by Kukui et al.[19] ((9 ± 3) × 10^{-11} cm^3 $molecule^{-1}$ s^{-1} at 298 K and P = 200−400 Torr). We also found that the present overall rate coefficient for the PSIA + $^{\bullet}OH$ reaction at 298 K is underestimated by ∼9 times with respect to the theoretically calculated MSIA + $^{\bullet}OH$ reaction reported by González-García et al.[18] with a rate coefficient value of ∼7.7 × 10^{-10} cm^3 $molecule^{-1}$ s^{-1} at 298 K. This difference is mostly due to the transition-state barrier height for the H-atom abstraction from the −OH moiety of MSIA being found to be 6.8 kcal mol^{-1} below that of the starting reactants (calculated at the CCSD(T)/IB//mPW1K/MG3S level). This clearly suggests that the transition-state barrier height for the abstraction of the H-atom from the −OH moiety of PSIA is ∼2.0 kcal mol^{-1} higher in energy as compared to the same reaction involved in the MSIA + $^{\bullet}OH$ reaction.[18]

3.6. Branching Ratios. The branching ratios for the different reaction paths contributing to the overall reaction in the studied temperatures between 200 and 320 K and at 1 atm are reported in Table S10 of the Supporting Information. Each reaction path contribution to the overall reaction was calculated from the ratio of individual reaction path rate coefficients and the overall rate coefficients at the corresponding temperature. The branching ratios provided in Table S10 are expressed as percentage contributions for each reaction path to the overall reaction. The highest contributor to the overall reaction is the abstraction of the H-atom from the −OH moiety of PSIA via TS7 to form $CH_3CH_2CH_2S(O)_2$ (P4) + H_2O, with a contribution from 70.7% at 200 K to 89.0% at 320 K. The contribution of the $^{\bullet}OH$ addition reaction path via TS8 to the overall reaction was found to decrease with increasing temperature, with a contribution of from 18% at 200 K to 2% at 320 K. This suggests that the $^{\bullet}OH$ addition reaction is important only under lower temperature conditions. The behavior of reactions having a negative temperature dependence has been described for various reaction systems. Singleton and Cvetanovic[51,52] observed a negative temperature dependence for the O (^3P)-initiated reactions with *cis*-$CH_3CH{=}CHCH_3$, $(CH_3)_2C{=}C(CH_3)_2$, and $(CH_3)_2CHCH_3$. The results of these studies suggested the formation of O(^3P)-alkene complexes, which are formed before the transition state in the reaction path. The reaction of C_2H_4 + $^{\bullet}OH$ shows a negative activation barrier and, as a result, a negative temperature dependence.[53,54] A list of various reactions that show a negative temperature dependence was provided in a study by Alvarez-Idaboy et al.[48] and includes ethene + $^{\bullet}OH$, propene + $^{\bullet}OH$, methyl propene + $^{\bullet}OH$, *cis*-2-butene + $^{\bullet}OH$, and trichloroethene + $^{\bullet}OH$. Their study also reports that methyl propene + O(^3P), *cis*-2-butene + O(^3P), and 2,3-dimethyl-2-butene + O(^3P) exhibit negative temperature dependences.[48]

The contributions from the H-atom abstraction paths via TS2 and TS3 to the overall reaction were found to be 3.6−2.5% and 5.5−5.6% in the 200−320 K temperature range, respectively. All other remaining abstraction path contributions were ∼1−3 orders of magnitude smaller compared to the values of the reaction that proceeds via TS7. In addition, we estimated the total contribution from the abstraction channels to the overall reaction. It was found to range from 82% at 200

https://doi.org/10.1021/acsearthspacechem.1c00062
ACS Earth Space Chem. 2021, 5, 1498−1510

K to 98% at 320 K. The other remaining contribution was from the •OH addition channel.

3.7. Atmospheric Implications. The most plausible oxidation mechanism for the reaction of PSIA with OH radicals under atmospheric conditions is presented in Figure 6. The energetics, rate coefficients, and branching ratio data in the present work suggest that the PSIA + •OH reaction mainly proceeds via two paths: (i) abstraction of the H-atom from the OH moiety of PSIA as shown in eq 4, leading to the formation of $CH_3-CH_2-CH_2-S(O)_2$ + H_2O; and (ii) •OH addition to the sulfur atom of the sulfinyl group in PSIA as illustrated in eq 5, leading to the formation of the $CH_3-CH_2-CH_2-S(O)(OH)_2$ radical. For path (i), the formed $CH_3-CH_2-CH_2-S(O)_2$ radical undergoes unimolecular dissociation through C−S single bond fission to form sulfur dioxide (SO_2) and propyl (C_3H_7) radical products. Similarly, for path (ii), the $CH_3-CH_2-CH_2-S(O)(OH)_2$ radical product formed from eq 5 undergoes further dissociation via two reaction pathways: in the first, unimolecular elimination of a water molecule leads to the formation of $CH_3-CH_2-CH_2-S(O)_2$, which then proceeds to form SO_2 and propyl radical. In the second, the $CH_3-CH_2-CH_2-S(O)(OH)_2$ radical undergoes C−S single bond cleavage leading to the formation of sulfurous acid (H_2SO_3) and propyl radical. The formed propyl radical is expected to undergo further reaction with molecular oxygen ($^3O_2$), which is present in large concentrations in the atmosphere.[36,55] The fate of propyl radical in the presence of atmospheric oxygen has been reported in the literature.[55] It suggests that propyl radical interacts with $^3O_2$ to form a $CH_3-CH_2-CH_2-O-O^•$ (RO_2) radical adduct (see Figure 6), which then undergoes unimolecular decomposition to form propylene (C_3H_6) and hydroperoxyl radical (HO_2) as final products. Thus, the results overall indicate that the engagement of PSIA by •OH results in the formation of SO_2, propylene, HO_2, sulfurous acid, and water as final products.

We next estimated the atmospheric lifetime of PSIA with respect to its interaction with OH in the temperatures between 200 and 320 K and at 1 atm. The lifetime of any atmospheric molecule can be calculated using eq 8:

$$\tau = \frac{1}{k_{\mathrm{PSIA+OH}}[\mathrm{OH}]} \tag{8}$$

In eq 8, the overall bimolecular rate coefficient (in cm^3 $molecule^{-1}$ s^{-1}) for the PSIA + •OH reaction is represented as $k_{PSIA+OH}$ and the average tropospheric concentration of the OH radical is represented as [OH]. We calculated the atmospheric lifetimes of PSIA with OH radicals using the overall rate coefficients estimated in the present work and the average atmospheric concentration of [•OH] (1.0×10^6 molecules cm^{-3}).[16] The estimated atmospheric lifetime of PSIA was found to be ∼2−4 h in the studied temperature between 200 and 320 K at 1 atm. This suggests that the most important tropospheric sink for PSIA is its reaction with OH radicals.

We then calculated the global warming potential (GWP) for PSIA. This is an important parameter, which indicates the possible impact of PSIA on the atmosphere relative to the impact of the same amount of carbon dioxide (CO_2). This can be calculated using eq 9:

$$\mathrm{GWP_{PSIA}} = \frac{a\int_0^t e^{-t/\tau}d\tau}{\mathrm{AGWP_{CO_2}}} \tag{9}$$

In eq 9, the total radiative forcing (RF) (in W m^{-2} $ppbv^{-1}$) is represented as "a" and the time horizon (TH) is represented as "t". The total RF was calculated using the Pinnock method (eq 10),[56] with the vibrational frequencies (ν_k) and intensities (A_k) of the corresponding vibrational modes k in the spectral range of 500−1500 for the PSIA being obtained using M06-2X/aug-cc-PVTZ level calculations

$$a = \sum_k \mathrm{A}_k F(\nu_k) \tag{10}$$

The atmospheric lifetime (τ) of PSIA with respect to •OH was determined in the present study. The estimated values of GWP for PSIA are 0.137, 0.06, and 0.03 for THs of 20, 50, and 100 years, respectively. Therefore, a negligible contribution to global warming is expected from PSIA as compared to the same amount of CO_2. However, atmospheric oxidation of PSIA leads to the formation of SO_2, propylene, HO_2, sulfurous acid, and water vapor, which have the potential to contribute to global warming and formation of aerosols. It should be noted that SO_2 is a major product that originates from H-atom abstraction from the OH group of PSIA with OH radicals, leading to formation of the $CH_3-CH_2-CH_2-S(O)_2$ radical. The formed $CH_3-CH_2-CH_2-S(O)_2$ radical then undergoes unimolecular dissociation via C−S single bond fission. Thus, the SO_2 product does not originate from direct elimination of SO_2 from the PSIA. The oxidation of SO_2 in the gas phase[57,58] and in the atmospheric aqueous phase[59−61] is the main source of tropospheric sulfuric acid. The other important product in the oxidation of PSIA is sulfurous acid, which is also an important intermediate in sulfuric acid formation.[62−64] In the atmosphere, sulfuric acid plays a critical role due to its contribution to new particle formation[65] and acid rain.[58] Thus, the products formed in the PSIA + •OH reaction may have a significant effect on climate, the environment, and human health. The results of the present study further expand our understanding of terrestrial sources of sulfur and their contribution to the atmospheric sulfur burden.

4. CONCLUSIONS

The atmospheric oxidation mechanism of the PSIA with •OH reaction was investigated at the CCS(D)T/aug-cc-pVTZ//M06-2X/aug-cc-pVTZ level of theory. The kinetics of all of the H-atom abstraction and •OH addition pathways involved in the PSIA + •OH reaction have been studied using the Mesmer kinetic code over a temperature range of 200−320 K and within the pressure range of 0.1−10 atm. The results indicate that the abstraction of H-atom from the OH moiety of PSIA is kinetically and thermodynamically more favorable compared to all of the possible paths. The branching ratios were estimated for all possible reaction pathways in the present work. The results reveal that the major reaction, which resulted in the formation of $CH_3CH_2CH_2S(O)_2$ + H_2O, contributes ∼88% to the overall reaction at 298 K and 1 atm. The atmospheric lifetime of PSIA with respect to OH radicals was estimated to be ∼2−4 h in the temperature range between 200 and 320 K and 1 atm. This suggests that this compound rapidly decomposes in the troposphere and exhibits a negligible impact on global warming. However, its decomposition products include SO_2 derived from C−S single bond fission in the $CH_3-CH_2-CH_2-S(O)_2$ radical, which is formed by H-atom abstraction from the OH group of PSIA. This product is not generated from the direct elimination of SO_2 from PSIA. The final products such as SO_2, propylene, HO_2, sulfurous

https://doi.org/10.1021/acsearthspacechem.1c00062
ACS Earth Space Chem. 2021, 5, 1498−1510

acid, and water vapor have the potential to contribute to global warming, acid rain, and formation of aerosols.

■ ASSOCIATED CONTENT

Supporting Information

The Supporting Information is available free of charge at https://pubs.acs.org/doi/10.1021/acsearthspacechem.1c00062.

Tables S1−S10 present the calculated total electronic energies including zero-point energy corrections, imaginary frequencies of various TSs as discussed in the text at the M06-2X level, rotational constants, vibrational frequencies, optimized geometries of all of the reactants, prereactive complexes, transition states, postreactive complexes and products, T1 diagnostic values, temperature- and pressure-dependent rate coefficients, tunneling contributions, and branching ratios; and Figures S1 and S2 show the potential energy profile for the direct elimination of sulfur dioxide (SO_2) from PSIA and IRC plot for transition states (TS11) (PDF)

■ AUTHOR INFORMATION

Corresponding Author

Rabi A. Musah − *Department of Chemistry, University at Albany—State University of New York, Albany, New York 12222, United States;* orcid.org/0000-0002-3135-4130; Email: rmusah@albany.edu

Author

Parandaman Arathala − *Department of Chemistry, University at Albany—State University of New York, Albany, New York 12222, United States*

Complete contact information is available at: https://pubs.acs.org/10.1021/acsearthspacechem.1c00062

Notes

The authors declare no competing financial interest.

■ ACKNOWLEDGMENTS

The financial support of the National Science Foundation (grant numbers 1310350 and 1710221) to R.A.M. is gratefully acknowledged. The authors thank the High-Performance Computing Center at the University at Albany-SUNY for their support.

■ REFERENCES

(1) Lomans, B. P.; van der Drift, C.; Pol, A.; Op den Camp, H. J. M. Microbial cycling of volatile organic sulfur compounds. *Cell. Mol. Life Sci.* **2002**, *59*, 575−588.

(2) Charlson, R. J.; Lovelock, J. E.; Andreae, M. O.; Warren, S. G. Oceanic phytoplankton, atmospheric sulphur, cloud albedo and climate. *Nature* **1987**, *326*, 655−661.

(3) Andreae, M. O.; Crutzen, P. J. Atmospheric aerosols: Biogeochemical sources and role in atmospheric chemistry. *Science* **1997**, *276*, 1052−1058.

(4) Faloona, I. Sulfur processing in the marine atmospheric boundary layer: A review and critical assessment of modeling uncertainties. *Atmos. Environ.* **2009**, *43*, 2841−2854.

(5) Boucher, O.; Moulin, C.; Belviso, S.; Aumont, O.; Bopp, L.; Cosme, E.; von Kuhlmann, R.; Lawrence, M. G.; Pham, M.; Reddy, M. S.; Sciare, J.; Venkataraman, C. DMS atmospheric concentrations and sulphate aerosol indirect radiative forcing: A sensitivity study to the DMS source representation and oxidation. *Atmos. Chem. Phys.* **2003**, *3*, 49−65.

(6) Bates, T. S.; Lamb, B. K.; Guenther, A.; Dignon, J.; Stoiber, R. E. Sulfur emissions to the atmosphere from natural sources. *J. Atmos. Chem.* **1992**, *14*, 315−337.

(7) Spiro, P. A.; Jacob, D. J.; Logan, J. A. Global inventory of sulfur emissions with 1°×1° resolution. *J. Geophys. Res.* **1992**, *97*, 6023−6036.

(8) Block, E.; Putman, D.; Zhao, S. H. Allium chemistry: GC-MS analysis of thiosulfinates and related compounds from onion, leek, scallion, shallot, chive, and Chinese chive. *J. Agric. Food Chem.* **1992**, *40*, 2431−2438.

(9) Oaks, D. M.; Hartmann, H.; Dimick, K. P. Analysis of sulfur compounds with electron capture/hydrogen flame dual channel gas chromatography. *Anal. Chem.* **1964**, *36*, 1560−1565.

(10) Arathala, P.; Musah, R. A. Computational study investigating the atmospheric oxidation mechanism and kinetics of dipropyl thiosulfinate initiated by OH radicals and the fate of propanethiyl radical. *J. Phys. Chem. A* **2020**, *124*, 8292−8304.

(11) Arathala, P.; Musah, R. A. Theoretical studies of the gas-phase reactions of s-methyl methanesulfinothioate (dimethyl thiosulfinate) with OH and Cl radicals: Reaction mechanisms, energetics, and kinetics. *J. Phys. Chem. A* **2019**, *123*, 8448−8459.

(12) Hofzumahaus, A.; Rohrer, F.; Lu, K.; Bohn, B.; Brauers, T.; Chang, C.-C.; Fuchs, H.; Holland, F.; Kita, K.; Kondo, Y.; et al. Amplified trace gas removal in the troposphere. *Science* **2009**, *324*, 1702−1704.

(13) da Silva, G. Oxidation of carboxylic acids regenerates hydroxyl radicals in the unpolluted and nighttime troposphere. *J. Phys. Chem. A* **2010**, *114*, 6861−6869.

(14) Li, S.; Matthews, J.; Sinha, A. Atmospheric hydroxyl radical production from electronically excited NO2 and H2O. *Science* **2008**, *319*, 1657−1660.

(15) Arathala, P.; Katz, M.; Musah, R. A. Reaction mechanism, energetics, and kinetics of the water-assisted thioformaldehyde + $\dot{O}H$ reaction and the fate of its product radical under tropospheric conditions. *Phys. Chem. Chem. Phys.* **2020**, *22*, 10027−10042.

(16) Prinn, R. G.; Huang, J.; Weiss, R. F.; Cunnold, D. M.; Fraser, P. J.; Simmonds, P. G.; McCulloch, A.; Harth, C.; Salameh, P.; Doherty, S.; et al. Evidence for substantial variations of atmospheric hydroxyl radicals in the past two decades. *Science* **2001**, *292*, 1882−1888.

(17) Tian, Y.; Tian, Z.-M.; Wei, W.-M.; He, T.-J.; Chen, D.-M.; Liu, F.-C. Ab initio study of the reaction of OH radical with methyl sulfinic acid (MSIA). *Chem. Phys.* **2007**, *335*, 133−140.

(18) González-García, N.; González-Lafont, À.; Lluch, J. M. Methanesulfinic acid reaction with OH: Mechanism, rate constants, and atmospheric implications. *J. Phys. Chem. A* **2007**, *111*, 7825−7832.

(19) Kukui, A.; Borissenko, D.; Laverdet, G.; Le Bras, G. Gas-phase reactions of OH radicals with dimethyl sulfoxide and methane sulfinic acid using turbulent flow reactor and chemical ionization mass spectrometry. *J. Phys. Chem. A* **2003**, *107*, 5732−5742.

(20) Flyunt, R.; Makogon, O.; Schuchmann, M. N.; Asmus, K.-D.; von Sonntag, C. OH-radical-induced oxidation of methanesulfinic acid. The reactions of the methanesulfonyl radical in the absence and presence of dioxygen. *J. Chem. Soc., Perkin Trans. 2* **2001**, 787−792.

(21) Glowacki, D. R.; Liang, C.-H.; Morley, C.; Pilling, M. J.; Robertson, S. H. MESMER: An open-source master equation solver for multi-energy well reactions. *J. Phys. Chem. A* **2012**, *116*, 9545−9560.

(22) Frisch, M. J.; Trucks, G. W.; Schlegel, H. B.; Scuseria, G. E.; Robb, M. A.; Cheeseman, J. R.; Scalmani, G.; Barone, V.; Petersson, G. A.; Nakatsuji, H. et al. *Gaussian 16*, revision B.01; Gaussian, Inc.: Wallingford, CT, 2016.

(23) Zhao, Y.; Truhlar, D. G. The M06 suite of density functionals for main group thermochemistry, thermochemical kinetics, noncovalent interactions, excited states, and transition elements: two new functionals and systematic testing of four M06-class functionals and 12 other functionals. *Theor. Chem. Acc.* **2008**, *120*, 215−241.

(24) Kendall, R. A., Jr.; Dunning, T. H.; Harrison, R. J. Electron affinities of the first-row atoms revisited. Systematic basis sets and wave functions. *J. Chem. Phys.* **1992**, *96*, 6796−6806.
(25) Kumar, M.; Francisco, J. S. Elemental sulfur aerosol-forming mechanism. *Proc. Natl. Acad. Sci. U.S.A.* **2017**, *114*, 864−869.
(26) Kumar, M.; Anglada, J. M.; Francisco, J. S. Role of proton tunneling and metal-free organocatalysis in the decomposition of methanediol: A theoretical study. *J. Phys. Chem. A* **2017**, *121*, 4318−4325.
(27) Parandaman, A.; Tangtartharakul, C. B.; Kumar, M.; Francisco, J. S.; Sinha, A. A computational study investigating the energetics and kinetics of the HNCO + (CH3)2NH reaction catalyzed by a single water molecule. *J. Phys. Chem. A* **2017**, *121*, 8465−8473.
(28) Ishida, K.; Morokuma, K.; Komornicki, A. The intrinsic reaction coordinate. An ab initio calculation for HNC→HCN and H−+CH4→CH4+H−. *J. Chem. Phys.* **1977**, *66*, 2153−2156.
(29) Gonzalez, C.; Schlegel, H. B. Reaction path following in mass-weighted internal coordinates. *J. Phys. Chem. A* **1990**, *94*, 5523−5527.
(30) Noga, J.; Bartlett, R. J. The full CCSDT model for molecular electronic structure. *J. Chem. Phys.* **1987**, *86*, 7041−7050.
(31) Lee, T. J.; Taylor, P. R. A diagnostic for determining the quality of single-reference electron correlation methods. *Int. J. Quant. Chem.* **1989**, *36*, 199−207.
(32) Lv, G.; Zhang, C.; Sun, X. Understanding the oxidation mechanism of methanesulfinic acid by ozone in the atmosphere. *Sci. Rep.* **2019**, *9*, No. 322.
(33) Wang, L.; Zhang, J. Ab initio study of reaction of dimethyl sulfoxide (DMSO) with OH radical. *Chem. Phys. Lett.* **2002**, *356*, 490−496.
(34) Dunning, T. H.; Peterson, K. A.; Wilson, A. K. Gaussian basis sets for use in correlated molecular calculations. X. The atoms aluminum through argon revisited. *J. Chem. Phys.* **2001**, *114*, 9244−9253.
(35) Carr, S. A.; Still, T. J.; Blitz, M. A.; Eskola, A. J.; Pilling, M. J.; Seakins, P. W.; Shannon, R. J.; Wang, B.; Robertson, S. H. Experimental and theoretical study of the kinetics and mechanism of the reaction of OH radicals with dimethyl ether. *J. Phys. Chem. A* **2013**, *117*, 11142−11154.
(36) Parandaman, A.; Kumar, M.; Francisco, J. S.; Sinha, A. Organic acid formation from the atmospheric oxidation of gem diols: Reaction mechanism, energetics, and rates. *J. Phys. Chem. A* **2018**, *122*, 6266−6276.
(37) Whelan, C. A.; Eble, J.; Mir, Z. S.; Blitz, M. A.; Seakins, P. W.; Olzmann, M.; Stone, D. Kinetics of the reactions of hydroxyl radicals with furan and its alkylated derivatives 2-methyl furan and 2,5-dimethyl furan. *J. Phys. Chem. A* **2020**, *124*, 7416−7426.
(38) Harding, L. B.; Klippenstein, S. J.; Jasper, A. W. Ab initio methods for reactive potential surfaces. *Phys. Chem. Chem. Phys.* **2007**, *9*, 4055−4070.
(39) Miller, W. H. Tunneling corrections to unimolecular rate constants, with application to formaldehyde. *J. Am. Chem. Soc.* **1979**, *101*, 6810−6814.
(40) Jasper, A. W.; Miller, J. A. Lennard−Jones parameters for combustion and chemical kinetics modeling from full-dimensional intermolecular potentials. *Combust. Flame* **2014**, *161*, 101−110.
(41) Bunkan, A. J. C.; Hetzler, J.; Mikoviny, T.; Wisthaler, A.; Nielsen, C. J.; Olzmann, M. The reactions of N-methylformamide and N,N-dimethylformamide with OH and their photo-oxidation under atmospheric conditions: experimental and theoretical studies. *Phys. Chem. Chem. Phys.* **2015**, *17*, 7046−7059.
(42) da Silva, G. Reaction of methacrolein with the hydroxyl radical in air: Incorporation of secondary O2 addition into the MACR + OH Master equation. *J. Phys. Chem. A* **2012**, *116*, 5317−5324.
(43) Bartis, J. T.; Widom, B. Stochastic models of the interconversion of three or more chemical species. *J. Chem. Phys.* **1974**, *60*, 3474−3482.
(44) Miller, J. A.; Klippenstein, S. J. Master equation methods in gas phase chemical kinetics. *J. Phys. Chem. A* **2006**, *110*, 10528−10544.
(45) Miller, J. A.; Klippenstein, S. J.; Robertson, S. H.; Pilling, M. J.; Green, N. J. B. Detailed balance in multiple-well chemical reactions. *Phys. Chem. Chem. Phys.* **2009**, *11*, 1128−1137.
(46) Robertson, S. H.; Pilling, M. J.; Jitariu, L. C.; Hillier, I. H. Master equation methods for multiple well systems: application to the 1-,2-pentyl system. *Phys. Chem. Chem. Phys.* **2007**, *9*, 4085−4097.
(47) Alvarez-Idaboy, J. R.; Mora-Diez, N.; Boyd, R. J.; Vivier-Bunge, A. On the importance of prereactive complexes in molecule−radical reactions: Hydrogen abstraction from aldehydes by OH. *J. Am. Chem. Soc.* **2001**, *123*, 2018−2024.
(48) Alvarez-Idaboy, J. R.; Mora-Diez, N.; Vivier-Bunge, A. A quantum chemical and classical transition state theory explanation of negative activation energies in OH addition to substituted ethenes. *J. Am. Chem. Soc.* **2000**, *122*, 3715−3720.
(49) Smith, I. W. M.; Ravishankara, A. R. Role of hydrogen-bonded intermediates in the bimolecular reactions of the hydroxyl radical. *J. Phys. Chem. A* **2002**, *106*, 4798−4807.
(50) Tyndall, G. S.; Orlando, J. J.; Wallington, T. J.; Hurley, M. D.; Goto, M.; Kawasaki, M. Mechanism of the reaction of OH radicals with acetone and acetaldehyde at 251 and 296 K. *Phys. Chem. Chem. Phys.* **2002**, *4*, 2189−2193.
(51) Singleton, D. L.; Cvetanovic, R. J. Temperature dependence of the reaction of oxygen atoms with olefins. *J. Am. Chem. Soc.* **1976**, *98*, 6812−6819.
(52) Singleton, D. L.; Furuyama, S.; Cvetanović, R. J.; Irwin, R. S. Temperature dependence of the rate constants for the reactions O(3P) + 2,3-dimethyl-2-butene and O(3P) + NO + M determined by a phase shift technique. *J. Chem. Phys.* **1975**, *63*, 1003−1007.
(53) Atkinson, R.; Perry, R. A.; Pitts, J. N., Jr. Rate constants for the reaction of OH radicals with ethylene over the temperature range 299−425 °K. *J. Chem. Phys.* **1977**, *66*, 1197−1201.
(54) Zellner, R.; Lorenz, K. Laser photolysis/resonance fluorescence study of the rate constants for the reactions of hydroxyl radicals with ethene and propene. *J. Phys. Chem. B* **1984**, *88*, 984−989.
(55) Huang, H.; Merthe, D. J.; Zádor, J.; Jusinski, L. E.; Taatjes, C. A. New experiments and validated master-equation modeling for OH production in propyl+O2 reactions. *Proc. Combust. Inst.* **2011**, *33*, 293−299.
(56) Pinnock, S.; Hurley, M. D.; Shine, K. P.; Wallington, T. J.; Smyth, T. J. Radiative forcing of climate by hydrochlorofluorocarbons and hydrofluorocarbons. *J. Geophys. Res.* **1995**, *100*, 23227−23238.
(57) Stockwell, W. R.; Calvert, J. G. The mechanism of the HO-SO2 reaction. *Atmos. Environ. (1967)* **1983**, *17*, 2231−2235.
(58) Calvert, J. G.; Lazrus, A.; Kok, G. L.; Heikes, B. G.; Walega, J. G.; Lind, J.; Cantrell, C. A. Chemical mechanisms of acid generation in the troposphere. *Nature* **1985**, *317*, 27−35.
(59) Harris, E.; Sinha, B.; van Pinxteren, D.; Tilgner, A.; Fomba, K. W.; Schneider, J.; Roth, A.; Gnauk, T.; Fahlbusch, B.; Mertes, S.; Lee, T.; Collett, J.; Foley, S.; Borrmann, S.; Hoppe, P.; Herrmann, H. Enhanced role of transition metal ion catalysis during in-cloud oxidation of SO2. *Science* **2013**, *340*, 727−730.
(60) Savarino, J.; Lee, C. C. W.; Thiemens, M. H. Laboratory oxygen isotopic study of sulfur (IV) oxidation: Origin of the mass-independent oxygen isotopic anomaly in atmospheric sulfates and sulfate mineral deposits on Earth. *J. Geophys. Res.: Atmos* **2000**, *105*, 29079−29088.
(61) Lagrange, J.; Pallares, C.; Lagrange, P. Electrolyte effects on aqueous atmospheric oxidation of sulphur dioxide by ozone. *J. Geophys. Res. Lett.* **1994**, *99*, 14595−14600.
(62) Sheng, F.; Jingjing, L.; Yu, C.; Fu-Ming, T.; Xuemei, D.; Jing-yao, L. Theoretical study of the oxidation reactions of sulfurous acid/sulfite with ozone to produce sulfuric acid/sulfate with atmospheric implications. *RSC Adv.* **2018**, *8*, 7988−7996.
(63) Boniface, J.; Shi, Q.; Li, Y. Q.; Cheung, J. L.; Rattigan, O. V.; Davidovits, P.; Worsnop, D. R.; Jayne, J. T.; Kolb, C. E. Uptake of gas-phase SO2, H2S, and CO2 by aqueous solutions. *J. Phys. Chem. A* **2000**, *104*, 7502−7510.

https://doi.org/10.1021/acsearthspacechem.1c00062
ACS Earth Space Chem. 2021, 5, 1498−1510

(64) Terraglio, F. P.; Manganelli, R. M. The Absorption of atmospheric sulfur dioxide by water solutions. *J. Air Pollut. Control Assoc.* **1967**, *17*, 403−406.
(65) Kulmala, M.; Pirjola, L.; Mäkelä, J. M. Stable sulphate clusters as a source of new atmospheric particles. *Nature* **2000**, *404*, 66−69.

https://doi.org/10.1021/acsearthspacechem.1c00062
ACS Earth Space Chem. 2021, 5, 1498−1510